Vacancy concentration in electron irradiated Ni_3Al

2004 J. Phys.: Condens. Matter 16 591

(http://iopscience.iop.org/0953-8984/16/4/008)

INSTITUTE OF PHYSICS PUBLISHING JOURNAL OF PHYSICS: CONDENSED MATTER

J. Phys.: Condens. Matter **16** (2004) 591–603 PII: S0953-8984(04)71876-7

Vacancy concentration in electron irradiated Ni_3Al

S Van Petegem[1,3], E E Zhurkin[2], W Mondelaers[1], C Dauwe[1] and D Segers[1]

[1] Department of Subatomic and Radiation Physics, Ghent University, Proeftuinstraat 86, BE-Gent, Belgium
[2] St Petersburg State Polytechnic University, K-89, Department of Experimental Nuclear Physics, Polytecknicheskaya street, 195251 St Petersburg, Russia

E-mail: steven.vanpetegem@psi.ch

Received 11 November 2003
Published 16 January 2004
Online at stacks.iop.org/JPhysCM/16/591 (DOI: 10.1088/0953-8984/16/4/008)

Abstract

In this paper we study the vacancy creation process in polycrystalline Ni_3Al under electron irradiation using positron annihilation lifetime spectroscopy. The complete irradiation experiment has been simulated using Monte Carlo and molecular dynamics techniques. This allows us to estimate the absolute vacancy concentration. Comparison with the experimental positron lifetimes results in a positron trapping coefficient for vacancies in Ni_3Al of $2.8 \times 10^{15}\ s^{-1}$. Furthermore the calculations show that 81% of the vacancies are located on the Ni sublattice. Using these results we discuss the vacancy concentration range in Ni_3Al for which positron annihilation lifetime spectroscopy is sensitive. Furthermore the annealing behaviour of the irradiated samples is investigated.

1. Introduction

Ni_3Al has been extensively studied because of its extraordinary mechanical properties at high temperatures and anomalous temperature dependence of the flow stress [1]. In contrast to many other interstitial compounds it exhibits solubility at both sides of the stoichiometric composition. Therefore no or few non-stoichiometric vacancies are produced.

Vacancies play an important role, for instance, in self-diffusion mechanisms, order–disorder phenomena and creep behaviour. Furthermore it has been well recognized that the ductility of Ni_3Al can be improved by adding a small amount of boron [2]. This is due to boron segregation at the grain boundaries. The segregation process will depend on the atomic structure in the grains, and vacancies play therein a crucial role. Vacancies can be induced by quenching or by electron irradiation. In this paper we will concentrate only on irradiation induced vacancies.

[3] Current address: NUM/ASQ, Paul Scherrer Institute, CH-5232 Villigen, Switzerland.

Table 1. Positron trapping coefficient for various materials.

Material	μ (10^{14} s^{-1} at.)	Method	References
Ni	22	Deformation[a]	[13]
Cu	1.2	Dilatometry	[10]
Ag	2.3	Dilatometry	[14]
Ta	4	Resistivity	[9]
Fe	11	Resistivity	[15]
$Fe_{82}Si_{18}$	2.9	Dilatometry	[16]
$Fe_{76}Si_{24}$	6.6	Dilatometry	[16]
$Fe_{65}Al_{35}$	56	Dilatometry	[16]

[a] Supposing a relationship between the vacancy concentration and the strain during deformation.

The irradiation response of Ni_3Al has been studied in the past by positron annihilation lifetime spectroscopy (PALS) [3–6]. PALS has proven to be a very sensitive tool to investigate the defect structure in solids. The lifetime of a positron in a solid reflects the local electron density seen by the positron, which depends on the size and concentration of the defects present in the material. A review on positron annihilation spectroscopy in metals can be found in [7, 8].

Positrons are localized in the attractive potential of defects. This is reflected by a distinct change in the annihilation parameters. One of those parameters is the positron trapping rate κ which is directly proportional to the defect concentration C:

$$\kappa = \mu C. \tag{1}$$

The scaling factor μ is called the positron trapping coefficient or specific trapping rate. It is the trapping rate for a unit atomic concentration of defects and it is the product of the positron velocity and the positron trapping cross section. The trapping coefficient is material and defect dependent. The experimental determination of μ is rather difficult because the absolute defect concentration, especially for low vacancy concentrations, is usually not well known. There exist a few methods to determine the absolute defect concentration. One can use residual resistivity measurements (see, for instance, [9]) or the differential-dilatometry method as a function of temperature (see, for instance, [10]) to determine the vacancy concentration. According to calculations of Nieminen and Laakonen [11], the value for μ for vacancies is of the order of 10^{14}–10^{15} s^{-1}. This agrees fairly well with values found in literature as shown in table 1 for various elements and alloys. For values and the determination of μ in vacancy-like defects in semiconductors we refer to [12] and references therein.

In this paper we determine the vacancy concentration in Ni_3Al after electron irradiation using Monte Carlo (MC) and molecular dynamics (MD) simulations. First we simulate the energy spectrum of the electrons that hit the target by MC simulations. Then we use a combination of MD and MC to model the creation and recombination of vacancies during electron irradiation. This leads to an estimation for the absolute vacancy concentration and consequently to an estimation of the positron trapping coefficient for vacancies in Ni_3Al. Based on these results we can determine the range of vacancy concentrations in Ni_3Al that can be examined by positron annihilation spectroscopy. Furthermore we discuss in short the annealing behaviour of the irradiation induced defects.

2. Techniques

2.1. Sample preparation and irradiation

Ni(4N) and Al(5N) were mixed in a ratio of 3:1 and melted using inductive heating in an Ar atmosphere. Disc-shaped samples with a diameter of 10 mm and a thickness of 0.5 mm were

cut using spark erosion. The samples were first mechanically etched using grinding paper and finished off with diamond paste with a grain size of 4 μm. Then the samples were chemically etched in mixture of equal volume parts of HNO_3, H_2SO_4 and H_2O. Finally they were annealed at a temperature of 1200 °C for 100 h to obtain homogeneous samples. Using EDX the final composition was found to be $Ni_{76}Al_{24}$, which means that the samples are hypostoichiometric. The Ni_3Al samples were irradiated at the LINAC (linear accelerator) facility at the Ghent University [17]. The initial energy of the electrons was 4 MeV. The electron beam had an intensity of 5 μA. The electron irradiation was done at a fluence of 10^{18} e^- cm^{-2}. Due to possible heating during the irradiation the samples were cooled in a water container.

2.2. Positron annihilation lifetime spectroscopy

The positron lifetime measurements were performed with a conventional fast–fast lifetime spectrometer (see, for example, [8]) with a resolution (FWHM) of about 220 ps using the sandwich arrangement. The positron source (about 0.4 MBq) was made by evaporating $^{22}NaCl$ onto a standard Kapton foil (7 μm thickness), which was then sealed with another foil. The positron lifetime spectra all contained more than 10^7 counts and were analysed using the multi-component program LT developed by Kansy [18].

Positron lifetime calculations were performed to support the experimental results. We have used the atomic superposition method (ATSUP), developed by Puska and Nieminen [7, 19]. The calculations were performed within the local density approximation (LDA) using the parametrization of the enhancement factor and correlation potential as proposed by Boroński–Nieminen [20], and within the generalized gradient approximation (GGA) as proposed by Barbiellini and co-workers [21].

A positron lifetime spectrum describes the probability distribution of the lifetime of the positrons. It consists essentially of exponential components. The number and decay of these components depends on the defect concentration, their type and distribution. Several models are used depending on the specific problem. The most simple model is the simple trapping model (STM) whose validity is restricted to the case where the defects are uniformly dispersed in the material (e.g. in the case of electron irradiation). When the defects are not uniformly dispersed, the diffusion trapping model (DTM) should be used, in which the complete time and space dependent positron diffusion equation should be solved.

The STM was introduced by Brandt [22] in trying to explain the second lifetime in alkali halides. The STM is based on the following assumptions:

- At time $t = 0$ all positrons are free.
- The positron trapping rate κ is proportional to the vacancy concentration C_v:

$$\kappa = \mu C_v \tag{2}$$

  where μ is the positron trapping coefficient.
- The positron may escape from a trap.

The decay curve is then given by

$$C(t) = N_T \sum_{i=0}^{N} I_i \lambda_i \exp(-\lambda_i t) \tag{3}$$

with I_i the fraction of positrons annihilating with decay rate λ_i and N_T the total number of annihilation events observed. The decay rate and intensity of each component in the spectrum can be calculated by solving a set of differential equations that describe the time evolution of each positron state. These equations can be solved for the general case of N types of defects

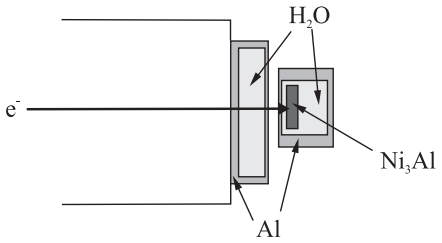

Figure 1. Schematic view of the LINAC set-up used for the EGS4 simulation of the irradiation of Ni_3Al (not to scale).

but here we will concentrate on the case of one type of defect and no detrapping. Then we get a lifetime spectrum with two components with annihilation rates given by

$$\lambda_1 = \lambda_f + \kappa \tag{4}$$

$$\lambda_2 = \lambda_v \tag{5}$$

with $\lambda_{f(ree)}$ and $\lambda_{v(acancy)}$ respectively the time independent annihilation rates for free and trapped positrons. The positron lifetime τ is defined as the inverse of the positron annihilation rate λ:

$$\tau_1 = \frac{1}{\lambda_1}, \qquad \tau_2 = \frac{1}{\lambda_2}, \qquad \tau_f = \frac{1}{\lambda_f}. \tag{6}$$

The following relations can be calculated:

$$\lambda_f = I_1\lambda_1 + I_2\lambda_2 \tag{7}$$

$$\tau_{av} = \frac{1 + \kappa\tau_v}{1 + \kappa\tau_f}\tau_f \tag{8}$$

$$\kappa = I_2(\lambda_1 - \lambda_2) \tag{9}$$

with τ_{av} the mean lifetime and $I_{1,2}$ the intensities of the two lifetime components. The validity of the trapping model can be tested by comparing $I_1\lambda_1 + I_2\lambda_2$ with the free annihilation rate according to equation (7). If this relationship is not valid then the STM cannot be used.

3. Results

3.1. Irradiation simulation

The complete irradiation experiment was simulated in two parts. First the energy spectrum and the spatial distribution of the electrons hitting the target was simulated using Monte Carlo simulations. These results then serve as an input for the calculation of the defect concentration in the sample in the region that can be detected by positron annihilation lifetime spectroscopy.

To calculate the dose and energy of the electrons absorbed by the samples, Monte Carlo simulations with the EGS4 code were performed [23]. The calculations are performed in a three-dimensional model of the electron accelerator, the exit window and the water container. A two-dimensional projection is shown in figure 1. A simulation without the water container was also performed.

The results of the EGS4 simulations are shown in figure 2. The electrons with an initial energy of 4 MeV lose a lot of their energy in the exit window, resulting in a rather broad energy spectrum with an maximum energy of 1.6 MeV and a mean energy of 1.1 MeV. The electrons further slow down in the cooling container, resulting in an energy spectrum with a maximum

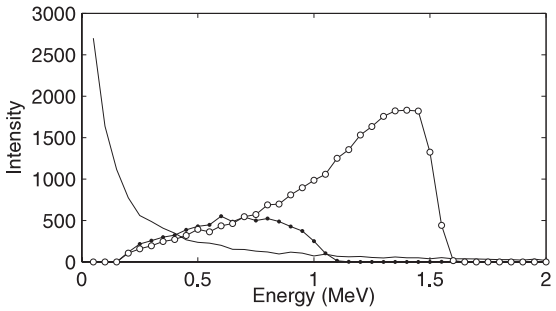

Figure 2. Results of the EGS4 simulations. The open circles represent the energy spectrum of the electrons after passing through the accelerator exit window. The energy spectrum of the electron that actually hit the target are represented by the solid circles. The solid curve shows the contribution of the photons that hit the target.

energy of 1.1 MeV and a mean energy of 0.65 MeV. Due to bremsstrahlung of the electrons in the exit window and the water container, the samples are also irradiated by a large amount of photons. Using a finite-element method the heating of the samples during irradiation was estimated. We used a thermal conductivity of 30 W K^{-1} m^{-1} [24] and an emissivity of 0.3, which is a lower limit for typical values of the emissivity in metals. These simulations show that without water cooling the temperature in the samples increases to several hundred degrees during the irradiation. In that case the created defects would anneal out immediately. Using water cooling the samples remain at room temperature as they are irradiated with a rather low electron current.

Now we can simulate the defect creation in the samples. Energetic electrons can give a part of their kinetic energy to a target atom due to elastic collisions. This primary knock-on atom (PKA) can give rise to a sequence of atomic collisions, leading to displacements of the target atoms and producing point defects (vacancies, interstitials and anti-sites). Most of them recombine spontaneously during a small time (about 500–1000 fs), and only a few defects remain stable. The minimal energy of PKAs, which is necessary to produce at least one stable Frenkel pair (so-called displacement threshold energy, E_d), strongly depends on the initial direction of the PKA. In respect to Ni_3Al, E_d values of Al and Ni PKAs were estimated by Gao and co-workers by means of MD [25]. The values vary between 17.3 and 70 eV for Ni primary recoils and 27.5 to 77.5 eV for Al primary recoils, depending on the initial direction of the PKA momentum. The maximum value of the energy transferred to a PKA atom due to an elastic collision with an electron (T_{max}) can be estimated for Ni and Al recoils according to relativistic kinematics (see, for instance, [26]). Typical values are $T_{max}(\mathrm{Ni}) = 73.42$ eV and $T_{max}(\mathrm{Al}) = 159.72$ eV for an electron with an energy of 1 MeV. Hence, electrons with this energy may produce stable defects in Ni_3Al.

In this study we check only the vacancy formation, as interstitials and anti-sites cannot be detected in Ni_3Al by positron annihilation spectroscopy. The simulations were performed in two stages. First we have performed MD simulations of several collision cascades initiated by PKAs with relevant energies T in the range $E_{d,min} < T < T_{max}$. This gives us for each PKA energy the average number of Ni and Al vacancies. In a second part we use a Monte Carlo method to simulate the PKA spectra under electron irradiation. Using the results of the first part we know the number of vacancies produced by each PKA. Averaging the number of vacancies over all PKA spectra results in the number of vacancies per incident electron and the final vacancy concentration.

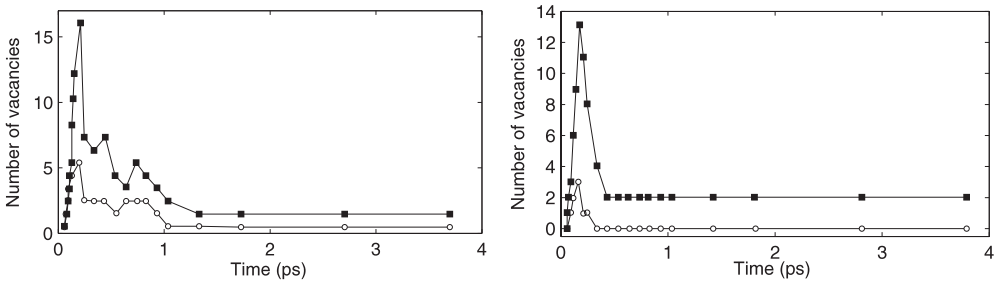

Figure 3. The time evolution of the number of Ni (■) and Al (○) vacancies during one PKA history created by Al PKA (left) and Ni (right) PKAs with initial energies of respectively 60 and 50 eV.

The simulations of the vacancy production by the PKA cascade were performed by means of a standard MD method [27]. We used the same potential as in [25] (which was designed in the frame of the second moment approximation of the tight binding model). The repulsive part of this potential is smoothly connected (via an exponential-cubic spline) to the Ziegler–Biersack–Littmark (ZBL) universal potential [28] at short interatomic distances. A computation box of 32 000 atoms ($20 \times 20 \times 20$ lattice distances) relaxed at zero temperature was used and periodic boundary conditions were applied. In addition, viscous damping forces were applied on the boundary atoms in order to provide the energy dissipation from the box. As is known, the unit cell of $L1_2$ Ni_3Al crystal contains four atoms. To treat all possible recoils, they were selected among these four atoms of one unit cell located close to the centre of the box. The simulations for Al and Ni recoils were performed separately. In the case of an Ni recoil, one of three possible atoms was selected at random. The initial direction of the recoil momentum through the spherical surface was selected at random from an isotropic distribution. The recoil history was followed up to 4 ps. The number of vacancies was estimated according the following criterion: a lattice site is considered as a vacancy if there are no atoms around within a sphere with a radius of $0.25 \times a_0/\sqrt{2}$, where a_0 is the lattice unit.

Examples of the evolution of the number of vacancies generated in the PKA collision cascade versus time are shown in figure 3. We consider a vacancy as a stable one if it exists after 4 ps tracing of the PKA history. For each selected value of the recoil energy we considered several histories (about 20 histories for Al recoils and 60 for Ni recoils). The final mean numbers of stable Ni and Al vacancies (averaged over different recoil directions) versus the initial PKA energy are shown in figure 4. These dependences were parameterized by linear fitting. It should be noted that the fluctuations of the number of vacancies generated by a PKA are quite large (typical values for the standard deviation are about 100% of the mean value).

First we will assume a constant electron energy of 2 MeV. The results can be directly compared with results reported in literature. The set of initial recoil atom energies (T) was generated by means of a standard Monte Carlo method (see, for instance, [29]) by using the Darwin and Rutherford relativistic differential cross-section with the McKinley and Feschbach correction to describe the recoil energy distribution in an electron–atom elastic collision [26]. Most of the collisions lead to a small energy transfer, and only 0.0089% of the collisions result in the creation of a PKA with an energy above the threshold energy ($T > E_{\mathrm{d,min}}$). The number of vacancies created by these PKAs was estimated according to the functional dependence obtained by the MD results. Then this value is averaged over the recoil energy spectra. The averaged number of vacancies per electron created in Ni_3Al can be found in table 2.

The bulk vacancy concentration (relative density) can be estimated as an average over the whole depth where we can detect vacancies. The implantation profile of high-energy positrons

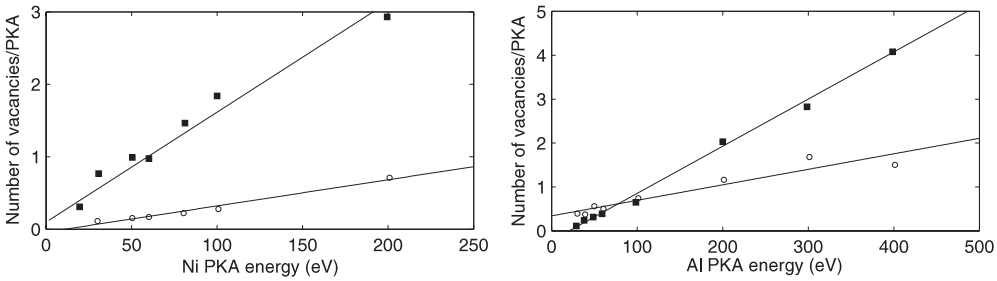

Figure 4. The average number of Ni (■) and Al (○) vacancies created by PKA as function of the PKA initial energy. The solid lines represent a linear fit.

Table 2. Number of vacancies created per electron and the vacancy concentration for 2 MeV electrons with a fluence of 10^{18} e^- cm^{-2} (C_v = vacancy concentration).

Atom	Number of vacancies/electron (10^{-5})	C_v (10^{-5} at.$^{-1}$)
Ni	6.954 ± 0.084	6.29
Al	1.478 ± 0.021	1.34

emitted from a radioactive ^{22}Na source into a solid can be described by an empirical law which was first found for electrons and which was later confirmed for positrons [30]. It states that the positron intensity $I(z)$ decays as

$$I(z) = I_0 \exp(-\alpha_+ z). \tag{10}$$

The mean implantation depth of the positrons is $1/\alpha_+$ and can be approximated as

$$\alpha_+ \approx 17 \frac{\rho \text{ (g cm}^{-3})}{E_{\max}^{1.43} \text{ (MeV)}} \text{ (cm}^{-1}) \tag{11}$$

where $E_{\max}$ is the maximum energy of the emitted positrons and ρ the density of the solid. In our case most of the positrons are stopped in the first 100 μm. On the other hand, the mean free path of 2 MeV electrons that can produce over-threshold PKAs is about 1.28 mm. Therefore, the ranges of electrons exceed to a great extent the depth of the analysed layer of the target. Hence, we can make the assumption that one electron may produce no more than one PKA in the selected layer of the target; in other words we consider the concentration of vacancies in the thin near-surface layer of the irradiated target. In that case we can apply the well known formalism to estimate the bulk vacancy concentrations in a thin layer during irradiation, for each kind of vacancies k (k = Ni, Al) separately:

$$N_{\text{vac}}(k) = \langle v_k(T) \rangle \Phi N_k \sigma_k \tag{12}$$

where $\langle v_k(T) \rangle$ is the mean number of vacancies created by one PKA and then averaged over the PKA energy spectra, Φ is the fluence of the electron irradiation, N_k is the partial concentration of kth kind of atoms (k = Ni, Al) and σ_k is the total cross-section of elastic scattering of an electron on an atom of kth kind. In the frame of our Monte Carlo techniques, in fact, we produce the mean vacancy concentration per one incident electron, ($\langle n_{\text{vac}}^{1e} \rangle_k$), which may be connected with the $\langle v_k(T) \rangle$ quantity by the following expression:

$$\langle n_{\text{vac}}^{1e}(k) \rangle = \langle v_k(T) \rangle \frac{N_k \sigma_k}{\Sigma_{\text{tot}}} \tag{13}$$

where Σ_{tot} is the macro cross-section of the target:

$$\Sigma_{\text{tot}} = \sum_k N_k \sigma_k. \tag{14}$$

Table 3. Number of vacancies created per incident electron and the final vacancy concentration calculated using as input the simulated energy spectrum of the electrons that hit the target (C_v = vacancy concentration).

Atom	Number of vacancies/electron (10^{-5})	C_v (10^{-6} at.$^{-1}$)
Ni	2.04 ± 0.14	1.43
Al	0.475 ± 0.042	0.34

Finally, our formula for the estimation of the relative bulk mean vacancy concentration is as follows:

$$C_v = N_{vac}(k)/N = \langle n_{vac}^{1e}(k)\rangle \frac{\Phi \Sigma_{tot}}{N} \tag{15}$$

where N is the atomic concentration of Ni_3Al ($N = 8.813 \times 10^{22}$ atoms cm^{-3}). For an initial electron fluence (Φ) of 10^{18} e$^-$ cm^{-2}, the relative bulk concentrations of vacancies are given in table 2. The total vacancy concentration is about $C_v = 7.6 \times 10^{-5}$ at.$^{-1}$.

In this case, most of the vacancies (81%) are Ni vacancies. This is in agreement with values reported in literature [3, 4]. The vacancy concentration is also in agreement with the estimation of the authors of [4], which was made in the frame of the simple Kinchin–Pease model (their estimation rescaled to the above mentioned fluence (10^{18} e$^-$ cm^{-2}) gives us the value $C_v = 9.4 \times 10^{-5}$ at.$^{-1}$).

Now we will consider the electron and photon energy spectrum that hit the target as calculated by EGS4. The calculations were performed by the same techniques as is described above. The only difference is that we have used a weighted average over all possible initial energies of the electrons, according to their energy spectra. The average number of Ni and Al vacancies per incoming electron is shown in table 3. The relative bulk vacancy concentration (relative density) can also be estimated. The mean free paths of electrons with an energy of 1, 0.5 and 0.1 MeV that can produce over-threshold PKAs are respectively 1.35, 1.50 and 1.90 mm. Again, our assumption is that one electron may produce no more than one PKA in the near-surface thin layer of the target seems to be reasonable. The concentration was estimated as an average over the energy spectra of the electrons. The formula for the relative bulk concentration of vacancies can be written as

$$C_v = \frac{N_{vac}(k)}{N} = \frac{\int \langle n_{vac}^{1e}(k, E_e)\rangle \varphi(E_e) \sum_{tot}(E_e) \mathrm{d}E_e}{N} \tag{16}$$

where $\varphi(E_e)$ is the energy spectrum of the electron fluence which is normalized to the actual fluence (Φ) of the electrons hitting the target:

$$\int \varphi(E_e)\, \mathrm{d}E_e = \Phi. \tag{17}$$

For the initial (total) electron fluence (Φ) of 10^{18} e$^-$ cm^{-2}, the actual fluence of electrons that hit the target is 0.0673×10^{18} e$^-$ cm^{-2}. The final concentrations C_v for Ni and Al vacancies created by the direct electron beam are listed in table 3. The total vacancy concentration is about 1.8×10^{-6} at.$^{-1}$.

The actual fluence of photons that hit the samples is about 0.108×10^{18} cm^{-2}, which is about 60% larger than the actual electron fluence. Therefore we also estimate the contribution of the photons to the defect creation. We have used the attenuation factors as given by [31]. The energy of the electrons created by the Compton effect is calculated by the Klein–Nischina formulae. The energy of the photo-electrons is approximated by the energy of the original photon (in fact we do not take the binding energy into account). It turns out that only 3.7% of

Table 4. Calculated positron lifetimes in Ni_3Al, Ni and Al using the atomic superposition method within the LDA and GGA scheme.

	LDA (ps)	GGA (ps)
Bulk Ni_3Al	105	114
Ni vacancy	176	183
Al vacancy	174	180
Ni–Al di-vacancy	193	201
Ni–Ni di-vacancy	196	198
Bulk Ni	97	109
Bulk Al	167	159

Table 5. Positron lifetime results on annealed and irradiated Ni_3Al.

Sample	τ_1 (ps)	τ_2 (ps)	I_1 (%)	I_2 (%)
Annealed	115	—	100	—
Irradiated	72	180	39.5	60.5

the photons interact in the analysed layer and most of these photons create electrons that have an energy which is too low to create a vacancy. The calculated vacancy concentration originating from the photon contribution is 1.00×10^{-9} at.$^{-1}$ and 2.45×10^{-10} at.$^{-1}$ respectively for Ni and Al vacancies. Compared to the vacancies created by the direct electron beam we can neglect this contribution.

3.2. Positron annihilation lifetime results

Table 4 shows the calculated positron lifetimes for delocalized positrons and positrons trapped in a mono-vacancy and a di-vacancy in Ni_3Al. No lattice relaxations were taken into account as their influence on the positron lifetime is restricted to a few picoseconds [32, 33]. Within LDA the lifetimes are systematically lower than within GGA. This is mainly due to the fact that LDA overestimates the contribution of the 3d electrons from Ni. This is in agreement with results found for elementary materials [21]. The results indicate furthermore that due to the limited resolution of positron lifetime spectroscopy Ni and Al vacancies can hardly be differentiated. The experimentally observed vacancy lifetime is then a weighted average of the single vacancy lifetimes.

The experimental positron lifetime results are shown in table 5. The positron lifetime of the well annealed Ni_3Al samples is 115 ps. According to table 4 we can assign this component to delocalized positrons. In fact the agreement with the bulk lifetime calculated using GGA is extremely good. This is a coincidence, as GGA slightly overestimates the bulk lifetime of Ni and underestimates the bulk lifetime of Al. Our experimental bulk lifetime is in agreement with values reported in literature by You [34], Wang [4] and Schaefer [35], and slightly higher than the lifetime of 110 ps reported by Shimotomai [3] and by Badura–Berger [36]. The lifetime spectrum for Ni_3Al after electron irradiation could be analysed into two lifetime components. According to table 4 we can attribute the second lifetime component $\tau_2 = 180$ ps to positrons trapped in the vacancies. This is in agreement with the results from Wang for vacancies created by electron irradiation and by quenching from 1100 °C [4]. The first lifetime τ_1 is smaller than the bulk lifetime and is according to equation (4) due to delocalized positrons.

The irradiated Ni_3Al samples were isochronally annealed in vacuum for 30 min at each temperature. After each annealing step a PAL measurement was performed at room temperature. Figure 5 shows the positron lifetime results as a function of the annealing

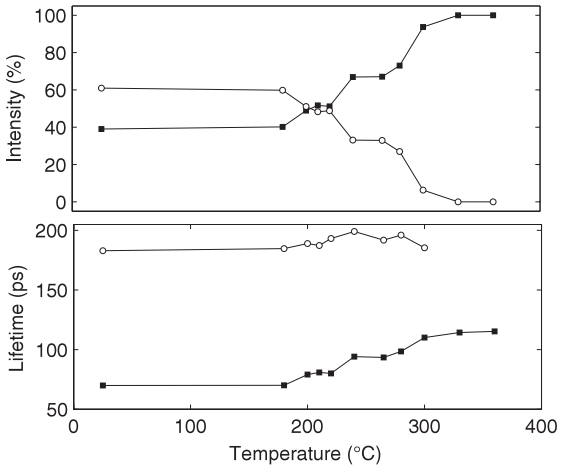

Figure 5. Positron lifetime results in irradiated Ni_3Al as a function of the annealing temperature. The lifetime and intensity of the first and second lifetime component are shown respectively by the full squares and open circles.

temperature. The lifetime spectra can all be analysed into two lifetime components. The intensity of the defect component (τ_2) starts to decrease at about 200 °C. The defect component completely disappears at 330 °C. This behaviour agrees with the observation by Wang and co-workers [4] except that in their case the defect component could be observed up to 500 °C. They argued that this would be due the formation of dislocation loops which are more stable than vacancies. At 220 °C the defect lifetime increases from 180 to 200 ps. According to the results of the positron lifetime calculations (see table 4) we can ascribe this to the formation of di-vacancies.

4. Discussion

Using equation (7) the bulk lifetime τ_f in the irradiated samples is about 113 ps, which agrees well with the experimental bulk lifetime. This is an indication that we can use the simple trapping model. Combining equations (1) and (9) together with the positron lifetime results of table 5 and the vacancy concentration obtained from the simulations, we obtain a specific trapping rate for vacancies in Ni_3Al of $\mu = 2.8 \times 10^{15}$ s^{-1} at. This is close to the specific trapping rate for Ni of 2.2×10^{15} s^{-1} at. as found by Dlubek *et al* [37, 13]. It is also in agreement with trapping coefficients for vacancies in other similar materials such as FeAl ($\mu = 1.6 \times 10^{15}$ s^{-1} at.) [38].

Using equations (4) and (9) we can estimate the upper and lower limit for the vacancy concentrations in Ni_3Al which can be detected by positron lifetime spectroscopy. Figure 6 shows the intensity of the vacancy component and the lifetime of the delocalized positrons as a function of the vacancy concentration. In the vacancy concentration range between 5×10^{-7} and 5×10^{-5} PAL is very sensitive to concentration variations. To estimate the lower limit we have performed a one- and two-component lifetime analysis on simulated spectra with 10^6 and 10^7 counts. The results are shown in figure 7. It shows that for spectra with 10^6 counts the normalized χ^2 does not significantly improve below a vacancy concentration of about 2×10^{-7} when we use a two-component fit instead of a one-component fit. In the case of 10^7 counts the lower limit shifts to about 8×10^{-8}. For lower concentrations we find the bulk lifetime of Ni_3Al.

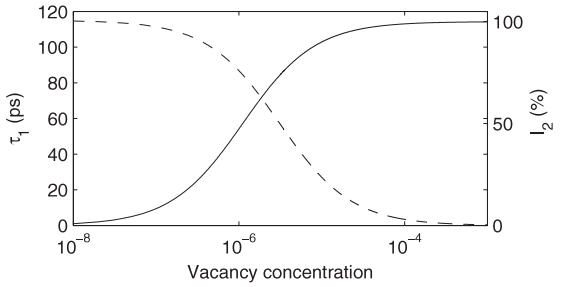

Figure 6. The intensity of the vacancy component (——) and the lifetime of the delocalized positrons (- - - -) as a function of the vacancy concentration.

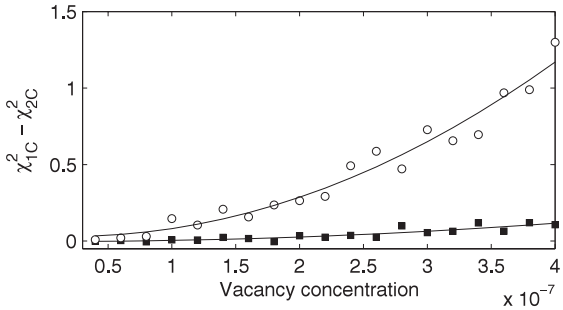

Figure 7. Difference in normalized χ^2 of a one- and two-component fit of a simulated spectrum with 1 million counts (■) and 10 million counts (○).

In principle vacancy concentrations up to 10^{-4} could be detected. But the first lifetime τ_1 then becomes very small (<20 ps). The best positron lifetime set-ups nowadays have a resolution (full width at half maximum) down to 120–140 ps (see, for instance, [39, 40]). In those cases one could go up to vacancy concentrations of somewhat less than 10^{-4}. Above these concentrations we can talk about saturation trapping; only the defect component can be resolved. In this regime positron lifetime spectroscopy can only be used to determine the size of the defects.

In the case of the well annealed samples we can conclude that the concentration of structural vacancies due to the deviation from the stoichiometric composition should be lower than 10^{-7}. This means that the deviations from stoichiometry are accommodated by substitutional antisite defects. This is in agreement with theoretical calculations on equilibrium point defect structures in Ni_3Al [33].

Using the simple trapping model we can calculate the vacancy concentration and the fraction of positrons that annihilate with bulk Ni_3Al as a function of annealing temperature. It should be noted that the intensities I_1 and I_2 are not the fractions of positrons annihilating from the bulk and from the defect state. These fractions are given by

$$\begin{aligned} \eta_f &= \int_0^\infty \lambda_f n_f(t)\,dt = \frac{\lambda_f}{\lambda_f + \kappa} \\ \eta_v &= \int_0^\infty \lambda_v n_v(t)\,dt = \frac{\kappa}{\lambda_f + \kappa}. \end{aligned} \tag{18}$$

For the calculations of the vacancy concentration we should take into account that the positron trapping coefficient for di-vacancies is larger than for vacancies. According to calculations

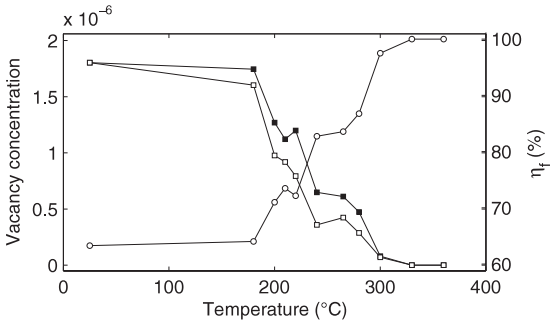

Figure 8. Vacancy concentration and fraction of positrons that annihilate with bulk Ni_3Al as a function of the annealing temperature. The fraction of positrons annihilating from the delocalized state is shown by the open circles. The vacancy concentration calculated by the trapping coefficient for vacancies is displayed by the solid squares. The corrected vacancy concentration calculated using equation (19) is represented by the open squares.

of Nieminen and Laakonen [11] for small defect clusters containing N vacancies the trapping coefficient scales directly to the size of the defect:

$$\mu_{N\mathrm{V}} \approx N\mu_{1\mathrm{V}} \tag{19}$$

with $\mu_{1\mathrm{V}}$ the positron trapping coefficient of a vacancy. Positron lifetimes between 180 and 200 ps can be due to several possible defects. Wang and co-workers ascribed a defect component of 187 ps to Al vacancies at dislocation loops [4]. This component was found to be stable above 300 °C, which is not the case here. We believe that in our case the intermediate lifetime components are due to a mixture of a mono-vacancy and a di-vacancy component which cannot be separated reliably in the lifetime analysis. In this case we can use equation (19) to calculate the defect concentration. The results are shown in figure 8.

5. Conclusions

We have performed positron lifetime experiments on electron irradiated Ni_3Al. To determine the vacancy concentration we have simulated the whole irradiation and vacancy creation process by Monte Carlo and molecular dynamics techniques. The following features have been shown: (1) the energy spectrum of the electrons hitting the samples is rather broad, which has its influence on the calculation of the vacancy concentration;(2) 81% of the vacancies are Ni vacancies; and (3) photons have no significant influence on the vacancy concentration. A comparison between the simulations and experiments leads to a positron trapping coefficient for vacancies in Ni_3Al of 2.8×10^{15} s^{-1}at.

Acknowledgments

This research is part of the Interuniversity Poles of Attraction Program—Belgian State, Prime Minister's Office—Federal Office for Scientific, Technical and Cultural Affairs (IUAP 5/1). This work was furthermore supported by Fonds voor Wetenschappelijk Onderzoek-Vlaanderen (FWO). The authors thank Dr J Kuriplach for providing us with his ATSUP code. E E Zhurkin would like to thank Professor M Hou for the computer time provided from the Free University of Brussels.

References

[1] Devvi S C, Sikka V K and Liu C T 1997 *Prog. Mater. Sci.* **42** 177
[2] Liu C T, White C L and Horton J A 1985 *Acta Metall.* **33** 213
[3] Shimotomai M, Wang T and Doyama M 1983 *J. Nucl. Mater.* **116** 347
[4] Wang T, Shimotomai M and Doyama M 1984 *J. Phys. F: Met. Phys.* **14** 37
[5] DasGupta A, Smedskjaer L C, Legnini D G and Siegel R W 1987 *Mater. Sci. Forum* **15–18** 1213
[6] Deng W, Xiong L Y, Lung C W, Wang S H and Guo J T 1997 *Intermetallics* **5** 265
[7] Puska M J and Nieminen R M 1994 *Rev. Mod. Phys.* **66** 841
[8] Hautojärvi P and Corbel C 1995 Positron spectroscopy in solids *Proc. Int. School of Physics Enrico Fermi Course CXXV* ed A Dupasquier and A P Mills Jr (Amsterdam: Institute of Physics Publishing) p 491
[9] Schaefer H E, Valenta P and Maier K 1979 *Positron Annihilation* ed R R Hasiguti and K Fujiwara (Sendai: The Japanese Institute for Metals) p 509
[10] Kluin J E and Hehenkamp T 1991 *Phys. Rev.* B **44** 11597
[11] Nieminen R M and Laakonen J 1979 *Appl. Phys.* **20** 181
[12] Krause-Rehberg R and Leipner H S 1997 *Appl. Phys.* A **64** 457
[13] Dlubek G, Brümmer O and Hensel E 1976 *Phys. Status Solidi* a **34** 737
[14] Kluin J E and Hehenkamp T 1991 *Mater. Sci. Forum* **105–110** 1329
[15] Vehanen A, Hautojärvi P, Johansson J, Yli-Kauppila J and Moser P 1982 *Phys. Rev.* B **25** 762
[16] Broska A, Wolff J, Franz M and Hehenkamp T 1999 *Intermetallics* **7** 259
[17] Mondelaers W, Van Laere K, Goedefroot A and Van den Bossche K 1996 *Nucl. Instrum. Methods* A **368** 278
[18] Kansy J 1996 *Nucl. Instrum. Methods* A **374** 235
[19] Puska M J and Nieminen R M 1983 *J. Phys. F: Met. Phys.* **13** 333
[20] Boroński E and Nieminen R M 1986 *Phys. Rev.* B **34** 3820
[21] Barbiellini B, Puska M J, Korhonen T, Harju A, Torsti T and Nieminen R M 1996 *Phys. Rev.* B **53** 16201
[22] Brandt W 1967 *Positron Spectroscopy of Solids* ed A T Stewardt and L O Roellig (New York: Academic) p 155
[23] Nelson W, Hirayama H and Rogers D 1985 *The EGS4 Code System* (Stanford: Stanford Linear Accelerator Center)
[24] Miura S, Terada Y, Suzuki T, Liu C T and Mishima Y 2000 *Intermetallics* **8** 151
[25] Gao F, Bacon D J and Ackland G 1993 *Phil. Mag.* A **67** 289
[26] Lehman C 1977 *Interaction of Radiation with Solids and Elementary Defect Production* (Amsterdam: North-Holland)
[27] Zhurkin E E and Kolesnikov A S 2002 *Nucl. Instrum. Methods* B **193** 822
[28] Ziegler J F, Biersack J P and Littmark U 1985 *The Stopping and Range of Ions in Matter* (New York: Pergamon)
[29] Murata K and Kyser D 1987 *Advances in Electronics and Electron Physics* ed P W Hawkes (New York: Academic) p 176
[30] Brandt W and Paulin R 1977 *Phys. Rev.* B **15** 2511
[31] Berger M J and Hubbell J H 1987 *NBSIR 87-3597, XCOM: Photon Cross-Sections on a Personal Computer* (Gaithersburg, MD: National Institute of Standards and Technology)
[32] Van Petegem S, Kuriplach J, Hou M, Zhurkin E E, Segers D, Morales A L, Ettaoussi S, Dauwe C and Mondelaers W 2001 *Mater. Sci. Forum* **363–365** 210
[33] Fu C L and Painter G S 1997 *Acta Mater.* **45** 481
[34] Yoo M H, Sass S L, Fu C L, Mills J, Dimiduk D M and George E P 1993 *Acta Metall.* **41** 987
[35] Schaefer H E, Würschum R and Bub J 1992 *Mater. Sci. Forum* **105–110** 439
[36] Badura-Gergen K and Schaefer H E 1997 *Phys. Rev.* B **56** 3032
[37] Dlubek G, Brümmer O, Meyendorf N, Hautojärvi P, Vehanen A and Yli-Kauppila J 1979 *J. Phys. F: Met. Phys.* **9** 1961
[38] Wolff J, Broska A, Franz M, Köhler B and Hehenkamp T 1997 *Mater. Sci. Forum* **255–257** 593
[39] Bečvář F, Čížek J, Lešták L, Novotný I, Procházka I and Šebesta F 2000 *Nucl. Instrum. Methods* A **443** 557
[40] Saito H, Nagashima Y, Kurihara Y and Hyodo T 2002 *Nucl. Instrum. Methods* A **487** 612